Journal of Biomechanics 48 (2015) 585–591

Contents lists available at ScienceDirect

Journal of Biomechanics

journal homepage: www.elsevier.com/locate/jbiomech
www.JBiomech.com

Unraveling the relationship between arterial flow and intra-aneurysmal hemodynamics

Hernán G. Morales*, Odile Bonnefous

Medisys – Philips Research Paris, France

ARTICLE INFO

Article history:
Accepted 7 January 2015

Keywords:
Cerebral aneurysms
Hemodynamics
CFD
Wall shear stress
flow rate

ABSTRACT

Arterial flow rate affects intra-aneurysmal hemodynamics but it is not clear how their relationship is. This uncertainty hinders the comparison among studies, including clinical evaluations, like a pre- and post-treatment status, since arterial flow rates may differ at each time acquisition. The purposes of this work are as follows: (1) To study how intra-aneurysmal hemodynamics changes within the full physiological range of arterial flow rates. (2) To provide characteristic curves of intra-aneurysmal velocity, wall shear stress (WSS) and pressure as functions of the arterial flow rate. Fifteen image-based aneurysm models were studied using computational fluid dynamics (CFD) simulations. The full range of physiological arterial flow rates reported in the literature was covered by 11 pulsatile simulations. For each aneurysm, the spatiotemporal-averaged blood flow velocity, WSS and pressure were calculated. Spatiotemporal-averaged velocity inside the aneurysm linearly increases as a function of the mean arterial flow (minimum $R^2 > 0.963$). Spatiotemporal-averaged WSS and pressure at the aneurysm wall can be represented by quadratic functions of the arterial flow rate (minimum $R^2 > 0.996$). Quantitative characterizations of spatiotemporal-averaged velocity, WSS and pressure inside cerebral aneurysms can be obtained with respect to the arterial flow rate. These characteristic curves provide more information of the relationship between arterial flow and aneurysm hemodynamics since the full range of arterial flow rates is considered. Having these curves, it is possible to compare experimental studies and clinical evaluations when different flow conditions are used.

1. Introduction

Hemodynamics influences the arterial wall behavior and regulates the blood coagulation process (Wootton and Ku, 1999; Reneman et al., 2006). In cerebral aneurysms, hemodynamics has been related to their initiation, development and rupture (Gao et al., 2008; Xiang et al., 2011; Meng et al., 2013) and is known to affect endovascular therapies, such as flow divertion (Mut et al., 2014a; Pereira et al., 2013a).

To understand intra-aneurysmal hemodynamics, vascular morphology and arterial flow conditions have to be considered. Morphology defines unique characteristics of the studied system (arterial calibers, aneurysm size and shape, etc.), those measurable from medical images. Several morphological features have been described like size, shape, aspect ratio, and correlated with aneurysmal rupture (Ujiie et al., 2001; Xiang et al., 2011). In contrast, it is not clear how arterial flow conditions alter intra-aneurysmal hemodynamics.

Through computational fluid dynamics (CFD) simulations, it has been shown that intra-aneurysmal hemodynamics depends on the arterial flow rates. Inside aneurysms, flow patterns and quantitative variables, such as velocity and wall shear stress (WSS), vary if flow conditions change (Jiang and Strother, 2009; Marzo et al., 2011; McGah et al., 2014). Moreover, CFD-based studies have highlighted the importance of imposing patient-specific flow rates and have quantified the errors when derived boundary conditions are used (Marzo et al., 2011; McGah et al., 2014). Nevertheless, patient-specific measurements are limited to the temporal frame of the examination. In other words, patient-specific flow conditions are time-dependent measurements, because arterial flow rates change during patient's lifetime. An example of such flow rate variation is when resting or exercising (Poulin et al., 1999).

In the lack of flow measurements, a wide range of possible boundary conditions is available from the literature. Some of those conditions are based on the geometry, like an area–inflow relation (Cebral et al., 2008) or based on physiological conditions, like a WSS of 1.5 Pa at the inlet of the model (Reneman et al., 2006).

* Corresponding author. Tel.: +33 01 47 28 3610; fax: +33 01 47 28 3600.
E-mail address: hernan.morales@philips.com (H.G. Morales).

http://dx.doi.org/10.1016/j.jbiomech.2015.01.016
0021-9290/

Other flow conditions can be obtained from mean values over young and elder populations (Hoi et al., 2010; Ford et al., 2005). The variety of boundary conditions makes unfeasible the comparison among experimental studies, particularly those conducted with CFD.

Indeed, a better understanding of the relationship "arterial flow-aneurysm hemodynamics" is required. In clinical practice for example, the uncertainties in this relationship hinder the comparison among medical image sequences, since flow conditions may differ among image acquisition times (Chien and Viñuela, 2013; Pereira et al., 2013a). More precisely, an evaluation of endovascular device performance by functional imaging could be done during clinical interventions (Bonnefous et al., 2012), or to assess longitudinal studies with several follow-ups if the relationship arterial flow-aneurysm hemodynamics is known.

The purpose of this work is to unravel the relationship between arterial flow and intra-aneurysmal hemodynamics when the full physiological range of arterial flow rates is covered. Quantitative characterizations of the averaged intra-aneurysmal velocity, WSS and pressure are pursuit. A clear relationship "artery-aneurysm flow" allows the comparison among experimental studies and clinical observations under different flow conditions.

2. Materials and method

2.1. Materials

Fifteen aneurysms from ten patients were studied. All aneurysms were located in one of the internal carotid arteries (ICA), between the carotid siphon and the ICA bifurcation. Two aneurysms were terminal and 13 lateral. Depending or their size, four aneurysms were classified as small (size < 3 mm), five as medium (size between 3 mm and 5 mm) and six as large aneurysms (size > 5 mm). To visualize these aneurysms, volumetric images were acquired by an X-ray system (Allura Xper FD20 system of Philips Healthcare).

2.2. Surface and volumetric mesh generations

Vascular models of the cerebral arteries harboring the aneurysms were extracted after segmentation of the volumetric images. Then, these models were conditioned for CFD simulations, whose details can be found in Morales and Bonnefous (2014). Briefly, the surface meshes were cleaned and repaired with Ramesh (2011) and smoothed with MeshLab (2012). Then, the inlet was extruded and remodeled to obtain a circular cross section using the *Vascular Modeling Toolkit* (Antiga and Steinman, 2009). The SnappyHexMesh utility of OpenFOAM (2013) was used to generate volumetric meshes inside the fluid domains. Details of the implemented meshing strategy, which produces grid-independent CFD computation, can be found elsewhere (Morales and Bonnefous, 2014).

2.3. Numerical modeling

The continuity and Navier–Stokes equations of an incompressible Newtonian fluid were numerically solved with OpenFOAM (2013, v2.2.1). Blood density and viscosity were 1060 kg/m^3 and 0.0035 Pa s, respectively, knowing that viscosity changes are negligible inside cerebral aneurysms (Morales et al., 2013). Walls were considered as rigid with no slip boundary condition. Zero-pressure conditions were imposed at the outlets. A parabolic profile was set at the inlet as spatial condition. This velocity profile changes over time, following a generic pulsatile waveform (Fig. 1). This waveform was extracted from optical flow techniques applied on angiographic sequences (Bonnefous et al., 2012; Pereira et al., 2013a). The mean flow rate, $\overline{Q}$, of this generic curve was 4.08 ml/s, to match the mean value found in the literature (Hoi et al., 2010).

2.4. Full physiological range of arterial flow rates

Using magnetic resonance imaging, several studies measured the flow rates at the ICA. A range of $\overline{Q}$ from 0.5 ml/s to 6 ml/s was measured by Cebral et al. (2008) and a geometry-based flow rate was found, where $\overline{Q}$ can be derived from the inlet area. A $\overline{Q} \pm$ standard deviation (SD) $= 4.56 \pm 0.95$ ml/s was reported for a young population, and 4.08 ± 1.0 ml/s in an older adult group (Ford et al., 2005; Hoi et al., 2010). Finally, the physiological condition of WSS equal to 1.5 Pa can be used assuming Poiseuille flow (Reneman et al., 2006).

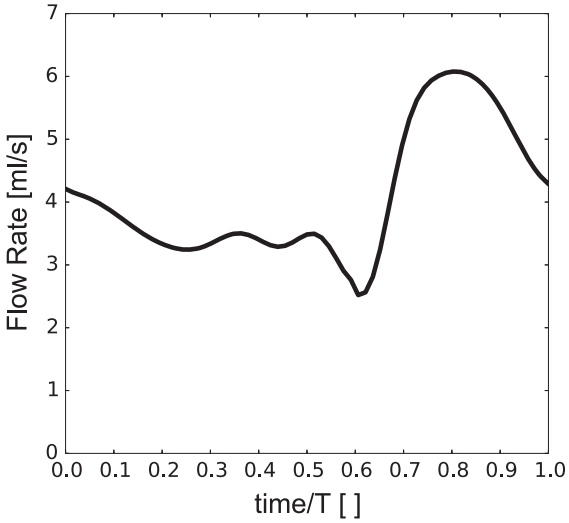

Fig. 1. Generic flow rate waveform ($\overline{Q} = 4.08$ ml/s). T is the cardiac period equal to 0.9 s.

To cover the reported physiological range of arterial flow rates and to satisfy those specific $\overline{Q}$s at the ICA, the generic waveform (Fig. 1) was scaled up and down. Eleven curves were created in total, whose $\overline{Q}$s roughly range from 0.5 ml/s to 6.3 ml/s. A thorough explanation of how these waveforms were derived can be found elsewhere (Morales and Bonnefous, 2014). The scaling preserves the shape of the generic waveform but varies $\overline{Q}$ among the generated waveforms.

2.5. Data analysis

From these pulsatile simulations, the spatial-averaged velocity magnitude (vel_{sa}), WSS (WSS_{sa}) and pressure (pre_{sa}) were calculated inside each aneurysm over a cardiac cycle. Afterwards, these variables were averaged over time and denoted as $\overline{\text{vel}}_{sa}$, $\overline{\text{WSS}}_{sa}$ and $\overline{\text{pre}}_{sa}$, respectively.

Maximum spatial-averaged WSS (maxWSS_{sa}), the oscillatory shear index (OSI) and the relative residence time (RRT) were also calculated. OSI and RRT were included due to their link with atherosclerosis initiation and promotion, whose formulations can be found elsewhere (He and Ku, 1996; Himburg et al., 2004; Xiang et al., 2011).

3. Results

Fig. 2A depicts temporal-averaged WSS distribution for 3 cases (3 aneurysms) for some $\overline{Q}$s. Temporal-averaged WSS magnitude increases with $\overline{Q}$ in all the vascular models, including the aneurysm walls. OSI distributions in 7 aneurysm models (3 cases) are shown in Fig. 2B. For these aneurysms, OSI seems to be stable from $\overline{Q} > \overline{Q}_3$, excepting for terminal aneurysms (case 2). Maximum OSI values in case 10 were located around the aneurysm bleb.

Spatiotemporal-averaged variables ($\overline{\text{vel}}_{sa}$, $\overline{\text{WSS}}_{sa}$ and $\overline{\text{pre}}_{sa}$), maxWSS_{sa}, OSI and RRT depending on $\overline{Q}$ are shown in Fig. 3. Higher flow rates increased the spatiotemporal-averaged variables and maxWSS_{sa}. OSI was almost constant in all cases, ranging from 0.004 to 0.08. Terminal aneurysms exhibited more variations in OSI than lateral aneurysms (see aneurysms of case 2). RRT decreased with increasing $\overline{Q}$.

3.1. Characteristic curves

To quantitatively characterize the intra-aneurysmal $\overline{\text{vel}}_{sa}$, $\overline{\text{WSS}}_{sa}$ and $\overline{\text{pre}}_{sa}$, linear and quadratic regression models were used. These particular regressions were applied to the data considering their behavior with respect to the arterial flow rate (Fig. 3). For intra-aneurysmal flow velocities, linear regression models were imposed